REPORT DOCUMENTATION PAGE

AFRL-SR-AR-TR-04-

0001

1. AGENCY USE ONLY (Leave blank)	2. REPORT DATE	3. REPORT TYPE AND DATES COVERED
	December 10,2003	Final Performance Report, 6/1/02 - 9/30/03

4. TITLE AND SUBTITLE

FLOW CONTROL OVER SWEPT, SHARP-EDGED WINGS AT LOW AND MODERATE ANGLES OF ATTACK

5. FUNDING NUMBERS

F49620-02-1-0291

6. AUTHOR(S)

Demetri P Telionis and Pavlos P. Vlachos

7. PERFORMING ORGANIZATION NAME(S) AND ADDRESS(ES)

Virginia Polytechnic Institute & SU
460 Turner Street, Suite 306
Blacksburg, VA 24060

8. PERFORMING ORGANIZATION REPORT NUMBER

430970

9. SPONSORING / MONITORING AGENCY NAME(S) AND ADDRESS(ES)

Air Force Office of Scientific Research
4015 Wilson Blvd.
Arlington, VA 22203

10. SPONSORING / MONITORING AGENCY REPORT NUMBER

11. SUPPLEMENTARY NOTES

12a. DISTRIBUTION / AVAILABILITY STATEMENT

Distribution Unlimited

12b. DISTRIBUTION CODE

13. ABSTRACT *(Maximum 200 Words)*

Active control of fully-separated flow over symmetric sharp-edged wings at high angles of attack is investigated. Experiments were carried out in a low-speed, open circuit wind tunnel, as well as a Mach 0.2, 6'x6' wind tunnel. Angles of attack from 3^0 to 21^0 were tested. Low-power input, unsteady excitation was applied to the leading edge of the wings. The actuation was introduced by the periodic oscillation of a 4-percent-chord flap placed on the suction side of the airfoil and facing the sharp edge. We also carried out experiments with pulsing jets and larger models at Reynolds numbers the order of one million. Our results indicate that blowing practically at the leading edge of a sharp airfoil is as effective as oscillating mini-flaps. Pressure measurements over all models show that the control increases the normal force coefficient by up to 40% to 70%. The application of flow control on sharp-edged aircraft wings could lead to improved maneuverability, short take–off and landing, innovative flight controls and weight reduction.

14. SUBJECT TERMS

Sharp-edge wings. Flow control, stalled wing control

15. NUMBER OF PAGES

27

16. PRICE CODE

17. SECURITY CLASSIFICATION OF REPORT	18. SECURITY CLASSIFICATION OF THIS PAGE	19. SECURITY CLASSIFICATION OF ABSTRACT	20. LIMITATION OF ABSTRACT
U	U	U	UL

FINAL REPORT

FLOW CONTROL OVER SWEPT, SHARP-EDGED WINGS AT LOW AND MODERATE ANGLES OF ATTACK

AFOSR GRANT NUMBER F49620-02-1-0291

Demetri P. Telionis and Pavlos P. Vlachos
Department of Engineering Science and Mechanics
Virginia Polytechnic Institute and State University
Blacksburg, VA 24061

Abstract

Active control of fully-separated flow over symmetric sharp-edged wings at high angles of attack is investigated. Experiments were carried out in a low-speed, open circuit wind tunnel, as well as a Mach 0.2, 6'x6' wind tunnel. Angles of attack from 3^0 to 21^0 were tested. Low-power input, unsteady excitation was applied to the leading edge of the wings. The actuation was introduced by the periodic oscillation of a 4-percent-chord flap placed on the suction side of the airfoil and facing the sharp edge. We also carried out experiments with pulsing jets and larger models at Reynolds numbers the order of one million. Our results indicate that blowing practically at the leading edge of a sharp airfoil is as effective as oscillating mini-flaps. Pressure measurements over all models show that the control increases the normal force coefficient by up to 40% to 70%. The application of flow control on sharp-edged aircraft wings could lead to improved maneuverability, short take–off and landing, innovative flight controls and weight reduction.

Introduction

Flying efficiently at high Mach numbers requires smaller, thinner, sharp-edged wings. Typically, these wings do not perform well during take-off and landing, requiring high speeds and long runways. Moreover the necessity for a small radar signature dictates the use of flat surfaces and sharp edges. The aerodynamic performance of sharp-edged wings decreases sharply for angles of attack greater than 5°, because the flow separates over the leading edge, with detrimental effects: increase in drag, decrease in lift, and reduction in aircraft maneuverability. Control of the separated flow over sharp wings can result in improved, time-averaged lift and drag characteristics. The present authors have demonstrated that indeed, this technique could improve the aerodynamics of sharp-edged wings at both moderate and high angles of attack[1].

In order to create the necessary flow disturbance, a small oscillating flap can be placed on the leading edge of a sharp-edged airfoil[1]. This pulsing flap creates an unsteady excitation at the leading edge, which is responsible for affecting the flow in the desired way. Previous work [2-5] has demonstrated that the maximum effect on separated flow is achieved when the actuation

frequency is near the vortex shedding frequency. But the flap or the disturbance it generates must penetrate the separated region in order to have any effect on the formation of vortices.

An alternative method of effecting flow control is by dynamic blowing and suction. Seifert, et al.[6] examined oscillatory blowing on the trailing edge flap of a NACA-0015 airfoil. They activated jets mounted in a 2-D slot located on the upper surface above the hinge of the flap. The airfoil was placed at an angle of attack of 20 degrees. Seifert et al. concluded that steady blowing had no effect on lift or drag. However, modulating blowing generated an increase in lift and cut the drag in half.

Synthetic-jet actuators can be used effectively achieve dynamic blowing and suction [7-8]. Synthetic-jet actuators based on piezoelectric devices are most efficient at the resonance frequency of the device and limited by the natural frequency of the cavity. Such actuators have proven very useful in the laboratory but may not be as effective in practice. Oscillating flaps are not limited in their frequency domain. Indeed Miranda et al.[1] demonstrated that an oscillating flap can generate a wide range of effective frequencies for the control of separated flow over a sharp-edged airfoil. But such devices may not be attractive to the aircraft designer. Recognizing these facts, Rao et al.[9] designed an actuator, which is essentially a small positive-displacement machine. The same group[10] later designed a similar device and tested a NACA0015 airfoil with rounded leading edges containing six reciprocating compressors, which were driven by two DC motors. These compressors/pistons created a synthetic jet (zero mean flux) at the leading edge of the airfoil. They found that flow separation control was demonstrated at angles of attack and free stream velocities as high as 25° and 45 m/s, respectively. These actuators may have overcome some of the problems faced by other designs but they are complex machines, requiring high-speed linear oscillatory motions and complex mechanical components.

The group of the present authors designed an actuator that would provide blowing amplitude independent of the disturbing frequency[11]. This actuator involves only a rotating component and the frequencies it produces are multiples of the frequency of the mechanical rotation. However, its design could not produce uniform spanwise flow and the amplitude of the flow oscillation was somewhat limited. In this report we describe a modification of our design, suggested originally by Beutner[12]. We have also mounted the new actuator on a sharp-edged airfoil and tested the effectiveness of the flow control system at moderate to high angles of attack.

So far, efforts have been reported to control the flow separation over airfoils with rounded leading edges, while here we report on the control of separated flow over sharp-edged airfoils. These techniques are equally applicable for the control of separated flows over rounded airfoils. There are two important differences between the actuator requirements for the two cases. First, the location of the actuators for the control of separation over rounded airfoils is not critical since the flow is still receptive to an external disturbance, whereas for the control of separated flow the actuation must interact with the free-shear layer. This fact dictates that the actuator of a sharp-edged wing must be as close as possible to the sharp edge, which leads to the second important difference. The direction of the actuation disturbance must be adjusted to lead the disturbance as much as possible in the direction of the free shear layer. Two additional important parameters are the $C\mu$ coefficient and frequency of the actuation. Different angles of attack and free stream velocities will require a wide variety of possible combinations. Being able to independently control both is a great challenge. These requirements may appear too stringent for the sharp- edged airfoils but on the other hand, they may provide some opportunities for robust control with minimal energy input. It is possible that free shear layers would be more receptive

to disturbances right at their initiation that is as close as possible to the sharp leading edge. Another similar situation is the control of asymmetric wakes over pointed bodies of revolution at incidence. In this case, minute disturbances very close to the apex can feed into the global instability of the flow and lead to very large wake asymmetries [13-14].

The next challenge that we need to face is the appropriate vectoring, so that a controlling jet does not shoot through the free shear layer. Several techniques for jet vectoring have been proposed. Most appropriate here to mention is the work of Smith and Glezer[15], who employ a synthetic jet to change the direction of a steady jet. In the present final report, we discuss the effectiveness of a passive method of jet vectoring.

A major step in the direction of achieving flow control of sharp-edge wings is to demonstrate that unsteady blowing near the leading edge is as effective as oscillating mini-flaps. Moreover, it is important to repeat such tests at higher Reynolds numbers, in order to demonstrate that the phenomena under consideration do not depend on the Reynolds number. Such tests have been carried out and the results are presented in this report and will also be included in a conference paper scheduled for presentation at the AIAA Aerospace Sciences Meeting in January 2004.

Actuator Design.

Zeiger et. al.[11] designed a jet mechanism appropriate for fitting as close as possible to the leading edge of a sharp-edged airfoil. This is essentially a wedge shown in Figure 1. A description of their design is repeated here for completeness. The actuation mechanism consists of two concentric cylinders shown in Figure 2. The inner cylinder contains two 1/16" wide slots, which span the length of the 7/16"-inch diameter inner brass tube. The inner cylinder rotates about a fixed axis inside a fixed outer cylinder created by the machined wedge. The inner cylinder is a brass tube, free to rotate on five bushings. One bushing was machined to fit snugly between the brass tubing and the machined leading edge at mid-span. This was done to eliminate possible warping of the tube during rotation. Two smaller bushings of the same type were placed in the inner brass tube. One was fixed to a pressure hose, so the cylinder could rotate independently of the fixed pressure line. The other was fixed to a motor drive shaft so that a small DC motor can drive the inner cylinder. The last two bushings are used to stabilize the tube in the machined leading edge but allowing rotation at the same time. All the bushings were press-fit to insure that the inner and outer cylinders are sealed tightly in order to maintain sufficient pressure in the inner cylinder.

This device operates as follows. The inner tube is continuously supplied with high-pressure air and is driven in rotation at a fixed frequency. In Figure 3, we show the inner-cylinder slots rotated by 90° with respect to the fixed slots, the closed position. When the slots of the inner rotating tube and the fixed outer tube match, the pressurized cavity releases air in the form of an unsteady jet. The flow is guided by the duct with width of 063", as shown in Figure 3 and released very close to the apex of the wedge. When the slots of the inner and the outer cylinder do not match, some air may leak between the two cylinders and find its way through the duct. The jet therefore has a non-zero mean component with an unsteady flow superimposed.

Following the suggestion of Beutner[12] , we modified our design. We added a larger, accumulator chamber right behind the rotating cylindrical plenum. Pressurized air is supplied to the accumulator chamber. The transfer of air from the accumulator to the rotating plenum is achieved again by alignment of slots on the latter. The design of the system and its attachment on the airfoil model are shown in Figure 4.

In this report, we present results of the performance of the new flow control mechanism. We also carried out wind tunnel and water tunnel tests to document the response of the aerodynamics of a sharp-edged airfoil to leading-edge flow control delivered with the unsteady jet actuator described.

Experimental Facilities

Wind-Tunnel Facilities and Models

The airfoil model was constructed in terms of a three profile sections and an aluminum skin, as shown in Figure 4. Pressure taps are distributed on the pressure and the suction side and are connected to PSI pressure scanners. A photograph of the model is shown in Figure 5 with the two skin surfaces peeled off. The airfoil spans the test section (51 cm) and the chord is 40 cm. The airfoil has a 12.6% thickness ratio.

Sixty-four pressure ports are distributed chordwise over the airfoil (32 each top and bottom) and are connected to ESP pressure scanners (Pressure Systems Inc.) Two 32-channel pressure scanners, with ranges of ±10" H2O and ±20" H2O are used to acquire data. The scanners are mounted inside the airfoil, allowing the pressure ports of the model to be connected to the pressure scanner with short tubes, which limit the phase difference and frequency attenuation between the measured and actual pressures. Tests indicated that for frequencies of 100 Hz or less, the delay in the response of the transducers leads to an uncertainty of less than 2% of the actual value[16]. The design of the scanners allows for full and zero-offset calibrations of the transducers without removing the scanners from the airfoil. The scanners interface with the data acquisition computer through a 12-bit A/D board and a separate scanner interface card. With this setup, the error in the pressure coefficients is no greater than 0.02.

The ESM wind tunnel is an open-circuit low-speed wind tunnel. The settling chamber has a contraction ratio of 5 to 1. The test section dimensions are 51 cm x 51 cm x 125 cm. Nylon screens and honeycombs placed near the entrance of the tunnel reduce the turbulence level. The tunnel can achieve free-stream velocities from 4 m/s to 20 m/s. The turbulence level does not exceed 0.51% at a free-stream velocity of 8.23 m/s, except for regions very near the tunnel walls. The flow across the test section has a velocity variation of less than 2.5%.

The second facility, the VA Tech six-foot subsonic wind tunnel, originally the NACA Stability Tunnel is classified as a continuous, closed-jet, single return, subsonic wind tunnel. It is equipped with 25-foot interchangeable, round and square test sections of six foot cross section. The tunnel is powered by a 600 hp DC motor driving a 14 foot propeller, providing a maximum speed of 230 ft/sec and a Reynolds number per foot up to $1.4X10^6$ in a normal 6'x6' configuration. Turbulence levels in this tunnel are extremely low, on the order of 0.05% or less. The turbulence level varies slightly with speed. The Tunnel is equipped with several balance systems, including six-component sting and strut strain gauge systems.

Water-Tunnel Facilities and Models

Time-Resolved Particle Image Velocimetry

Water tunnel experiments were carried out in the 2'x2' ESM Fluid Mechanics laboratory water tunnel. This facility is equipped with state of the art, in-house developed Time Resolved Digital Particle Image Velocimetry (TRDPIV). Our PIV system is based on a powerful laser (55 Watts), which is guided through a series of special mirrors and lenses to the area of interest and

is opened up to a laser sheet directed across the field. In the present case, the laser sheet is placed in the mid-span of the airfoil aligned parallel to the free-stream... The free stream velocity was 0.25 m/s with corresponding water tunnel free stream turbulence intensity approximately 1%. A traversing system allows adjusting the distance from the models to the laser sheet. The flow is seeded with neutrally buoyant fluorescent particles, which serve as flow tracers. The diameter of the particles is on the order of 100 microns such that the particles accurately follow the flow with no response-lag to any turbulent fluctuations. A CMOS video camera captures the instantaneous positions of the particles. The laser and the camera are synchronized to operate in dual-frame, single-exposure DPIV mode with sampling frequencies of 1000 Hz. This mode of operation allows very detailed temporal resolution, sufficient for resolving the turbulent flow fluctuations present in the wake.

The velocity evaluation is carried out using a multi-grid iterative DPIV analysis. The algorithm is based on the work by Scarano and Rieuthmuller[18]. In addition to their method we incorporated a second-order Discrete Window Offset (DWO) as proposed by Wereley and Meinhart[19]. This is a simple but essential component. Time-resolved DPIV systems are limited by the fact that the time separation between consecutive frames is the reciprocal of the frame rate, thus on the order of milliseconds. This value is relatively large compared with microsecond time-intervals employed by conventional DPIV systems. By employing a second order DWO we provide an improved predictor for the particle pattern matching between the subsequent iterations. Moreover, the algorithm employed performs a localized cross-correlation which, when compared to standard multi-grid schemes for resolving strong vortical flows was proven to be superior. Further details on the system, the algorithm and the associated error analysis can be found in Abiven and Vlachos[20] and Abiven et al.[21]

For the needs of the present study, the multigrid scheme was employed with a window hierarchy of 32-32-16-16-8 pixel^2 and a space resolution of 4 pixels/vector. Two different magnifications were employed resulting in 0.5 mm and 1mm space resolution. The overall performance of the method yield time resolution 1 milliseconds with sampling time up to 2 seconds and average uncertainty of the velocity measurement on the order of 10^{-3} m/s independently of the velocity magnitude. The vorticity distribution in the wake is calculated from the measured velocities using 4th order, compact, finite-difference schemes [16].

Sharp-Edge airfoil Water Tunnel Model

A first generation water tunnel SEA model has been designed and fabricated out of ABS plastic using a rapid-prototyping facility. This model is shown in Figure 6. Its internal chamber is connected with high-precision, computer-controlled gear pumps via the water supply connector shown in the Figure. The pumps allow the generation of pulsing jets with mean flow with unsteady blowing or synthetic jet actuation via blowing and suction action. The airfoil section is geometrically similar to the one fabricated for the wind-tunnel tests. The chord was 100 mm and the maximum thickness was approximately 15% of the chord. The span of the model was 220 mm while a uniform jet-exit slot width was 1mm. The geometry is similar to the one depicted in Fig. 3, with one side shorter by 5 mm than the other. Finally, end plates were installed at the tips of the model in order to assure two-dimensional flow and control of the end effects.

For the experimental results presented here, the Reynolds number based on the chord was Re=25,000. The airfoil was placed at an AOA=25 deg in order to generate a massively separated flow. Based on a Strouhal number of 0.2 the natural shedding frequency was estimated around 1Hz. The latter was chosen as the actuator frequency yielding $F^+=1$. The actuator generated a jet with zero offset and an amplitude of u_{jet}=0.15m/s with 50% duty cycle. The above numbers

result in a $C\mu$=0.006. Three cases will be presented here. First the flow of the pulsing jet alone, second the flow over the airfoil with no control and finally the flow with control. These cases were investigated using two different magnifications, first with the field of view covering the whole airfoil with 1 mm spatial resolution, and second with fine resolution of 0.5 mm zooming near the actuator jet.

Results

Wind-Tunnel Actuator Testing

To test the actuator design we mounted the assembled leading edge actuator in the test section of a wind tunnel aligned with a rake of four high-frequency-response Pitot tubes. The rake was connected to a HP digital signal analyzer, which was used to measure jet frequencies and amplitudes. It was mounted on three traversing scales so it could easily be displaced to obtain data at different locations downstream of the slotted nozzle.

Velocity profiles at different distances across the steady jet are plotted in Figure 7. We observe that the location of the maximum velocity is displaced upward, i.e. in the direction of the short side of the nozzle. This implies that there is a deviation of the direction of the jet away form the direction of the axis of the duct. Averaged profiles of the pulsed jet are presented in Figures 8, 9 and 10 for three driving frequencies. Now the vectoring of the jet is somewhat stronger. We attribute this vectoring tendency to the asymmetry of the nozzle. As shown in Figure 3, one side of the jet duct is much shorter than the other. As a result, the boundary layer on one side becomes a free shear layer before the other. Thus on one side, the free vorticity may start rolling, while the other side is constrained by the flat solid wall and vorticity retains its organization in the form of parallel flat layers. Rolled vortices may now generate regions of low pressure and induce changes of the direction of the jet. This is essentially a Coanda effect. Apparently, this effect is mild for steady flow. This is expected, because the distance the free shear layer has to travel before the other side becomes also free is short. In such a distance, no large vortical structures can grow. The situation is different with pulsing. An unsteady jet started from rest quickly rolls into two large vortices in two dimensions or a vortex ring in axisymmetric flow[22-25]. But in our case, the asymmetry of the two flat sidewalls, allows the formation of a large vortex on one side but forces vorticity to be confined in an attached boundary layer on the other. The vortex forming only on one side induces a low pressure as well as flow away from the long wall. A stronger vectoring away from the axis of symmetry of the wing and therefore a more effective disturbance will probably be introduced in the separated flow. In addition, the increase in frequency does not further change the velocity profiles with respect to the steady blowing case.

Time records of velocity distributions of the jet for steady and pulsed motions are presented in Figure 11 and the corresponding spectra are presented in Figure 12. We observe that with the same plenum pressure, the unsteady velocity magnitudes are considerably higher than their corresponding steady flow velocity magnitudes.

In Figure 13, we present preliminary results obtained with the instrumented wing in the ESM Wind Tunnel. This is only a 20"X20" and therefore the blockage generated with our model is very large. These tests were carried out only to confirm qualitatively the effects of unsteady jet blowing actuation. In this figure we display the averaged pressure distributions over the suction and the pressure side of the airfoil for two different $C\mu$ values. The blowing amplitude is sustained constant and the $C\mu$ is adjusted by changing the free-stream velocity. In the average, the pressure distributions start resembling those over rounded airfoils sustaining attached flow.

For the higher Cμ case the control clearly increases the maximum suction. The suction strength is stronger on the leading edge part of the airfoil and it decreases towards the trailing-edge.

TRDPIV Water Tunnel Actuator Testing

This section presents the flow characteristics of the actuator jet and its interaction with the incident flow. The mechanism of perturbing an unstable mode in the flow in order to roll-in an organized and coherent vortical structure is documented with detailed spatial and temporal resolution. Comparisons between the global development of the flow with and without control are presented.

First, we zoomed in the neighborhood of the edge, documenting the development of the actuator jet. A space resolution of 0.5mm and temporal resolution of 1millisec was employed. Figure14 shows a time sequence of 10 instantaneous velocity fields and vorticity distributions within one cycle of the actuator pulse. The frames are spaced apart by 0.02 seconds. The initiation of the jet in the flow is shown in Figure 14-a. The formation of a pair of counter-rotating vortices continues in figure 14-b. Clearly, the slot geometry allows the generation of an asymmetric free-shear flow, which is confined on the lower side but it is allowed to accumulate vorticity and roll into a strong vortex that dominates the upper side of the slot. This is further manifested in figures c-e where the clockwise vortex grows in strength as well as in size. As a result, it induces a velocity to the jet that favors the upper-side thus effectively vectoring the actuator jet at an angle with respect to the jet exit direction. At this point the dimensionless time is approximately $t^*=15$ which means that the jet reaches a steady state condition and the corresponding L/H assumes very large values. Thus, a jet parallel to the slot forms with the classic shear layer vortices illustrated in Figures 14f-i.

The striking feature of this sequence is that the impulsive character of the jet favors the formation of a starting vortex on the upper side of the slot. This is the equivalent of a passive control mechanism introduced by the slot geometry, directing the jet at an angle with respect to the airfoil chord. This is a favorable feature, because once the jet will interact with the incident free stream, it will curve and align with the leading edge shear layer.

In fact, this argument is confirmed in the following sequence of instantaneous flow fields, where the interaction of the jet with the free-stream flow is presented. Initially, figures 15-a and b show the separated shear layer before the initiation of the controlling jet. Clear shear layer instabilities are developing and the flow is highly disorganized. In figure 12-c the initiation of the jet in the flow generates a clockwise rotating vortex with its locus approximately at $x=0.13$ $y=0.1$. This vortex induces a downward velocity to the shear layer vortices thus triggering a vortex pairing and the roll-up of a strong coherent vortex (Figures 15 c-d). In the subsequent figures (e-h), we witness one coherent vortex that interacts strongly with the airfoil increasing the vorticity (positive) levels and potentially inducing a pressure drop that will increase the suction and thus the lift. Remarkably, the dimensionless time required for vortex formation on the suction side is on the order of $t^*=15$ which appears to be the same as the time required for the pulsing jet to reach a steady state. Figures 15 i-j demonstrate that as the strength of the pulsing jet decays, the strength of the suction vortex reduces.

The above-described sequence of figures reveals the mechanism for controlling separated flow. The jet vortex interacts with the natural instabilities, forcing them to grow through a vortex pairing process and subsequently form a strong coherent vortex that increases the suction. The continuation of the blowing within the pulsing cycle does not appear to further enhance the process. The results indicate that the starting vortex is predominantly affecting the flow. This

allows us to speculate that a more efficient way to manage the flow by minimizing the input would be by reducing the duty cycle of the pulsing for the same $C\mu$.

Finally, we performed experiments in order to document the global character of the flow. The field of view extended over the whole chord of the airfoil. Time average streamlines and vorticity distributions are shown in Figure 16. By comparing the uncontrolled cases (left) with the controlled ones (right), we do not observe any radical differences. In both cases, in a time-averaged sense, the flow is attached after the mid-chord. This may be due to the thickness of the airfoil. The suction vortex appears to be more coherent and concentrated. Moreover, it is clear that when the control is on, the trailing edge vortex is stronger and closer to the airfoil. This can only be attributed to increase in the strength of the leading edge vortex, since the interaction of the two will bring them closer and initiate the alternate vortex shedding pattern.

High-Reynolds Number Tests

Tests were then carried out in the VA Tech Stability Wind Tunnel. The model was equipped with flat end plates to reduce as much as possible the end effects. This technique generates fields that are closer to two-dimensional motions than if the model were to be attached to the tunnel walls. This is because boundary layers growing on the walls are thick and interact with the flow near the roots of the airfoil, giving rise to horseshoe vortices. With our 16"-chord model we ran tests very near a Reynolds number of one million. Tests were carried out at angles of attack of 3^0 up to 21^0, in increments of 3^0 .Average pressure measurements for these angles of attack are shown in Figs. 17 through 23. For all these cases, the actuation frequency was set at the estimated value of the natural shedding frequency.

For $\alpha=3^0$ (Fig. 17), we observe a peculiar sharp drop near the leading edge on the suction side. Cahill et al.[26] also observed this behavior, even though their model had a thickness ratio of .08 which is lower than the ratio of 0.12 of our model. We believe that this is due to a separated bubble very near the leading edge. Our control mechanism is not very effective at $\alpha=3^0$ and 6^0, a behavior we expected, since the flow is attached over most of our relatively think wing. But our control actuation lowers the pressure levels in the very front of the airfoil, where the separation bubble resides. Our actuation is not effective even at $\alpha=9^0$, as shown in Fig. 19. But at $\alpha=12^0$ (Fig. 20), we observe some significant departures from the no-control case. The comparison of the data of these two Figures clearly indicates that the flow at $\alpha=9^0$ displays the classical behavior of attached flow over airfoils. The suction pressure has its extreme values very near the leading edge. The reader should be cautioned to the fact that we are plotting here the negative of the pressure coefficient, and thus the extreme suction value is the minimum. Suction is reduced as we move towards the trailing edge. Now for $\alpha=12^0$, the no-control case indicates a flat pressure distribution on the suction side. The flow is fully separated. And yet, much like the case of oscillating mini-flaps, unsteady blowing at the leading edge brings the pressure distributions closer to those of attached flow, namely, the pressure is lowered near the leading edge and rises near the trailing edge. This is deceiving, because the flow is separated. It is only in the average that the pressure distribution is similar to the distribution of attached flow. The effect is more pronounced with higher levels of C_μ.

In figures 21, 22 and 23, we observe that at higher angles of attack, the effect of flow control is not as large and in fact it is progressively reduced as the angle of attack is increasing. It may be possible to achieve greater reductions on the suction pressure with larger values of C_μ, but we were not able to run such tests.

We calculated the lift coefficients by integrating the pressures over the suction and pressure side of the wing. The results are presented in Table 1, for the three values of C_μ. The benefit on the lift coefficient is not as large as those obtained earlier in our small wind tunnel. We attribute this discrepancy to the large blockage values imposed by the small cross-section of our ESM Wind Tunnel.

Table 1. C_L for all conditions

AOA	No control	C_μ = 0.003	C_μ = 0.01	C_μ = 0.03	Increase in C_L
3	0.4230	0.4150	0.4354	0.4458	5%
6	0.6420	0.6690	0.6277	0.6405	-0.23%
9	0.8410	0.8047	0.8046	0.8571	1.91%
12	0.5719	0.5905	0.6086	0.7344	28.41%
15	0.3881	0.3801	0.4131	0.5117	31.85%
18	0.3538	0.3424	0.3874	0.4395	24.22%
21	0.3618	0.3587	0.3884	0.4116	13.76%

Cahill and his co-workers[26] carried out many experiments with sharp-edged wings with and without flaps. Direct comparison of their data with the present results is not appropriate, since their thickness coefficient was 0.06 and ours is 0.12. Yet, we find it useful to make some comparisons anyway. In Fig. 24 we observe a remarkable agreement for $\alpha=6^0$. But for $\alpha=9^0$ (Fig. 25), the deviation is considerable. We believe there is a reasonable explanation for this discrepancy. The data clearly indicate that even without flow control, the flow over our airfoil is nearly attached. The pressure distribution resembles those over rounded-leading-edge airfoils. This can be attributed to the wing's thickness. With only 6% thickness that airfoil of Ref. 26 is practically a flat plate and thus at $\alpha=9^0$, the flow over such a wing is separated, displaying a nearly flat pressure distribution. At $\alpha=12^0$, the flow over the thick airfoil is separatred as well. But now, flow control can greatly influence the pressure distribution as shown in Fig. 26.

Conclusions

We describe in this report an actuator that can generate a pulsing jet along a slotted nozzle. The basic feature of this device is that it can generate pulsing flow without any mechanical oscillating parts, like a pulsating wall or an oscillating piston. A common limitation that the device can overcome is in the range of frequencies achieved. The pulsing jet frequency is controlled by the rotation of the inner cylinder and the number of the slots machined along its circumference. The frequency of rotation of a well-balanced cylinder can be increased easily, but more important is the fact that the pulse jet frequency is a multiple of the rotation frequency. The factor of the multiplicity is the number of the slots machined along the circumference. In the case presented here, there are two lines of slots, machined apart by 180 degrees and therefore the frequency of jet pulsing is double the motor frequency.

Our experimental data indicate that the efficiency of this actuator is practically independent of the frequency. The modified design proved that uniform and more powerful pulsing jets could be generated along the span of the airfoil. This means that the device is an

excellent candidate for a robust flight actuator, where the required frequency is changing with aircraft speed and the angle of attack.

Focusing in the neighborhood of the controlling jet revealed that the asymmetry of the walls induces a significant vectoring effect that guides the disturbance in the direction of the leading edge free shear layer. Moreover, we found that with control on or off, the flow over the suction side of the airfoil consists of many unsteady vortices that roll and drift downstream. However, in the control case, vortices form a little closer to the airfoil surface and appear to be more energetic.

Finally, we demonstrated for the first time, that unsteady blowing right at the leading edge of a sharp-edged airfoil allows the management of the separated flow leading to averaged pressure distributions that correspond to higher lift and lower drag.

References:

1. Miranda, S., Telionis, D., Zeiger, M., 2001, "Flow Control of a Sharp-Edged Airfoil," AIAA Paper No. 2001-0119, Jan. 2001.
2. Zhou, M. D., Fernholz, H. H., Ma, H. Y., Wu, J. Z., Wu, J. M., 1993, "Vortex Capture by a Two-Dimensional Airfoil with a Small Oscillating Leading-Edge Flap," AIAA Paper 93-3266.
3. Hsiao, F. B., Liang, P. F., Huang, C. Y., 1998, "High-Incidence Airfoil Aerodynamics Improvement by Leading-edge Oscillating Flap," J. of Aircraft. Vol. 35, No. 3, pp. 508-510.
4. Hsiao, F. –B., Wang, T.-Z., Zohar, Y., 1993, "Flow separation Control of a 2-D Airfoil by a Leading-Edge Oscillating Flap," Intl. Conf. Aerospace Sci. Tech., Dec. 6-9, 1993, Tainan, Taiwan.
5. Wu, J. Z., Lu, X. Y., Denny, A. G., Fan, M., Wu, J. M., 1998, "Post-stall flow control on an airfoil by local unsteady forcing", *Journal of Fluid Mechanics* 371, pp. 21-58.
6. Seifert, A., Bachar, T., Koss, D., Shepshelovich, M., Wygnanski, I., 1993, "Oscillatory Blowing: A Tool to Delay Boundary-Layer Separation," AIAA Journal. Vol. 31, No. 11, pp. 2052-2060.
7. Amitay M, Smith B. L. and Glezer, 1998, "Aerodynamic flow control using synthetic jet technology", AIAA Paper 98-0208.
8. Smith B. L. and Glezer A., 1998, "The formation and evolution of synthetic jets" Phys. of Fluids 10, 2281-2297.
9. Rao, P. Gilarranz, J.L., Ko, J. Strgnac, T. and Rediniotis, O.K., "Flow Separation Control Via Synthetic Jet Actuation", AIAA Paper 2000-0407, 38th Aerospace Sciences Meeting and Exhibit, Reno, Nevada, January 2000.
10. Gilarranz, J. L., Rediniotis, O. K., 2001, "Compact, High-Power Synthetic Jet Actuators For Flow Separation Control," AIAA Paper 2001-0737.
11. Zeiger, M.D., Gerlach, J.M., Vlachos, P.P. and Telionis, D.P.2002, " Frequency-and Amplitude-Independent Flow Controller for Sharp-Edged Wings. AIAA Paper no, 02-0969
12. Beutner, Thomas, 2002, private communication.
13. Zeiger, M.D. and Telionis, D.P. 1997 "Effect of Coning Motion and Blowing on the Asummetric Side Forces on a Slender Forbody" AIAA Paper No 97-0549.
14. Zilliac, G.G., Degani, D. and Tobak, M. 1990 "Asymmetrci Vortices on a Slender Body of Revolution" AIAA Journal, pp 667-675.
15. Smith B.L. and Glezer, A. 2002, "Jet Vectoring Using Synthetic Jets", Journal of Fluid Mechanics, Vol 458, pp. 1-34.

16. Rediniotis, O.K., "The Transient Development of Vortices Over a Delta Wing," Ph.D. Dissertation, VPI & SU, Oct. 1992
17. McManus, K., Magill, J., 1996, "Separation Control in Incompressible and Compressible Flows using Pulsed Jets," AIAA Paper 96-1948.
18. Scarano, F. and Rieuthmuller, M. L. (1999): Iterative multigrid approach in PIV image processing with discrete window offset. Experiments in Fluids, 26, 513-523.
19. Wereley ST, Meinhart CD (2001): Second-order accurate particle image velocimetry. Experiments in Fluids, 31, pp. 258-268.
20. C. Abiven, P. P. Vlachos (2002): "Super spatio-temporal resolution, digital PIV system for multi-phase flows with phase differentiation and simultaneous shape and size quantification", Int. Mech. Eng. Congress, Nov. 17-22, 2002, New Orleans, LA
21. C. Abiven, P. P. Vlachos and G. Papadopoulos (2002): "Comparative study of established DPIV algorithms for planar velocity measurements", Int. Mech. Eng. Congress, Nov. 17-22, 2002, New Orleans, LA
22. Didden, N. 1979: "On the Formation of Vortex Rings: Roling Up and Productions of Circulation." Z. Angew. Math.Phys. Vol 30, pp101-106.
23. Glezer, A. 1998: " The Formation of Vortex Rings". Phys. Fluids, Vol 31, pp. 3532-3542.
24. Gharib, M., Rambod, E. and Shariff, K. 1998:"A Universal Time Scale for Vortex Ring Formation", J.Fluid Mech., Vol 360, pp. 121-140.
25. Glezer, A. and Amitay, M. 2002: 'Synthetic Jets", Ann. Rev. Fluid Mech., Vol. 34, pp. 503-529.
26. Cahil F, Underwood, W. J., Nuber R. J., and Cheesman G. A., (1953) :"Aerodynamics forces on symmetrical circular-arc airfoils with plain leading-edge and plain trailing-edge flaps", NACA Report 1146.

Personnel Supported:

Jose Rullan	Graduate student, VA Tech
Pavlos P. Vlachos	Assistant Professor, VA Tech
Demetri P. Telionis	Professor, VA Tech

Some of the work described here will be part of the PhD dissertation of Mr. Rullan, who will continue working on this project. He is expected to complete the requirements for his PhD by May of 2005.
Dr. Vlachos started working on this project as a research assistant professor. In the Spring of 2003, Dr. Vlachos interviewed for a tenure track position at the Department of Mechanical Engineering at VA Tech. Since August 2003, Dr. Vlachos is serving as an assistant professor in this Department. Dr. Vlachos will continue working on this project.

Publications:

1. "Post-Stall Flow Control of Sharp-Edged Wings via Unsteady Blowing", by J.Rullan, P.P.Vlachos, D.P.Telionis and M.D. Zeiger. Presented at the 41st AIAA Aerospace Sciences Meeting, AIAA Paper No 2003-0062, January 2003.

2. " Flow Control of Unswept and Swept, Sharp-Edged Wings via Unsteady Blowing", by J.Rullan, P.P.Vlachos, D.P.Telionis and M.D. Zeiger, accepted for presentation at the 42st AIAA Aerospace Sciences Meeting, January 2004.

AFRL Point of Contact:

Dr. Carl Tilmann Carl.Tilmann@wpafb.af.mil
One of the PI's (DPT) visited Dr. Tilmann in the Fall of 2002 and presented a seminar at AFRL. The same PI had informal discussions in January 2003 with Dr. Tilmann at the AIAA meeting in Reno. Copies of the AIAA paper and the new submitted abstract were also mailed to him.

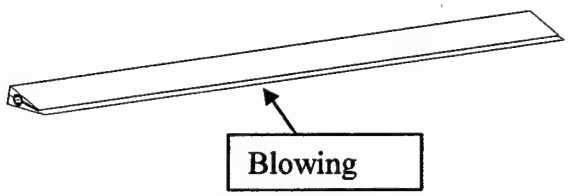

*Figure 1:*Machined Sharp Leading Edge with Flow Control Device

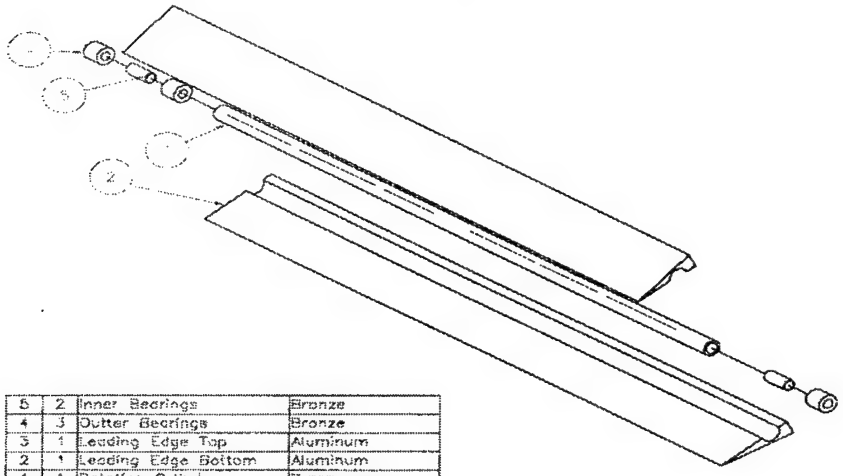

ITEM	QTY	NAME	MATERIAL
5	2	Inner Bearings	Bronze
4	3	Outter Bearings	Bronze
3	1	Leading Edge Top	Aluminum
2	1	Leading Edge Bottom	Aluminum
1	1	Rotating Cylinder	Brass

Parts List

*Figure 2:*Exploded View of Flow Control Device

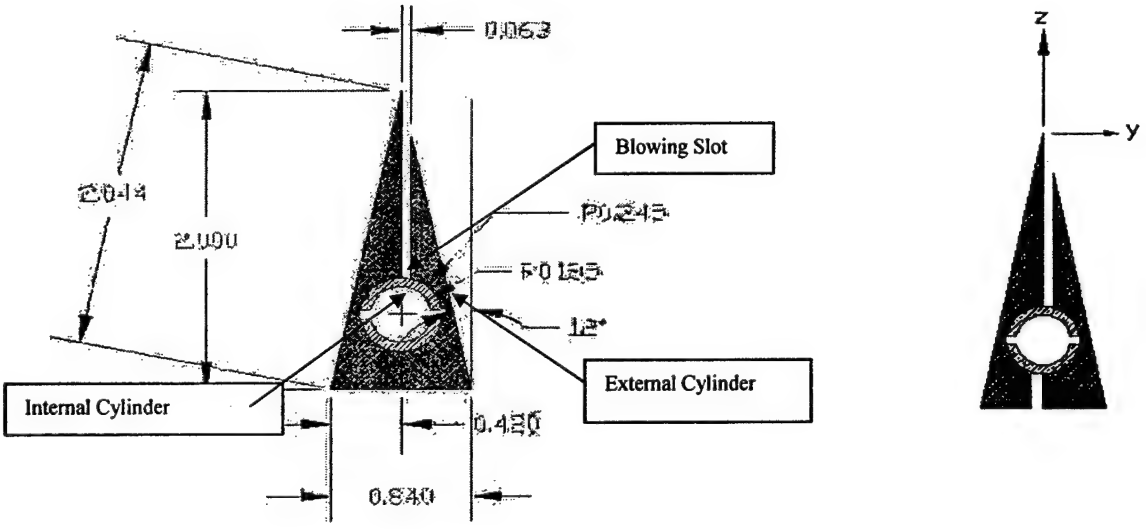

*Figure 3:*Cross Section of Flow Control Device.

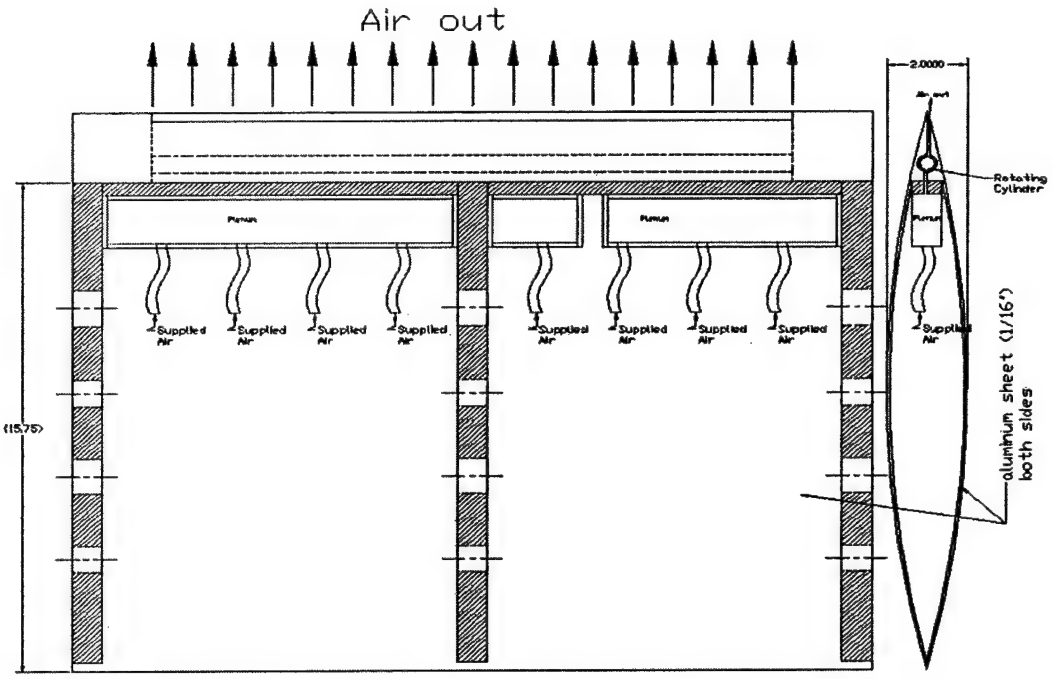

Figure 4: Drawing of the sharp-edged airfoil with the leading –edge attachment that houses the rotating cylinder and the accumulator chamber.

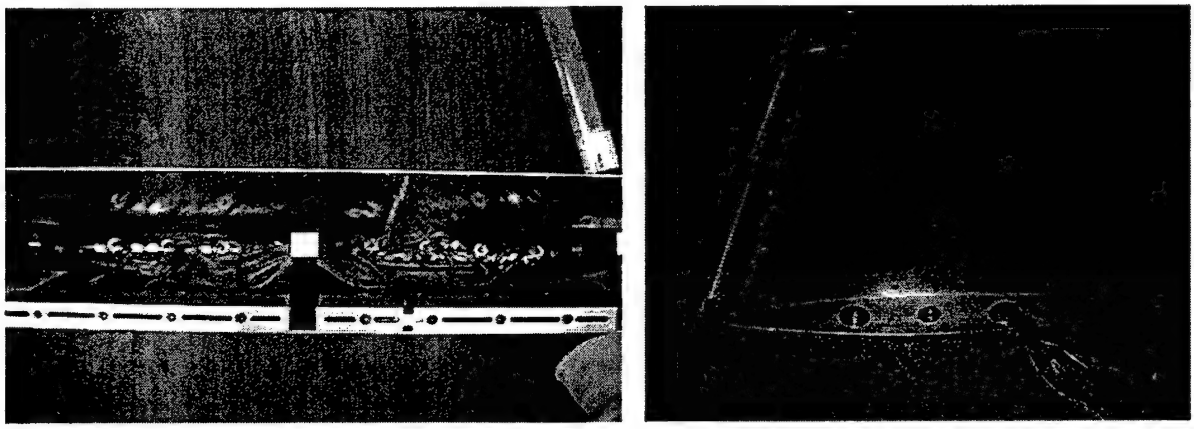

(a) (b)

Figure 5: Photograph of the inside of the airfoil, showing the pneumatic flow control system and the pressure tubes. The skin of the model is open in this photograph. It bolts down on the bulkheads to form the shape of a sharp-edged airfoil.

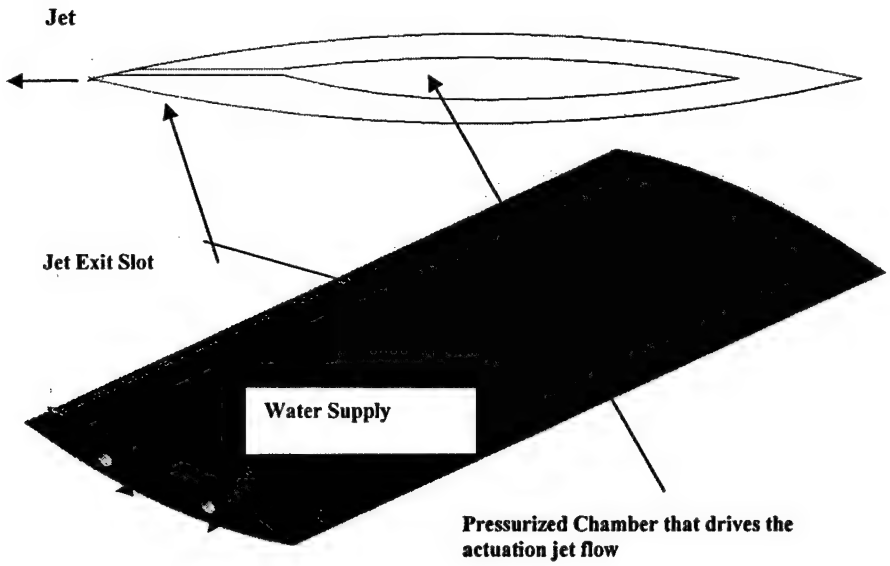

Figure 6: Profile and rendered 3-D view of the water tunnel model

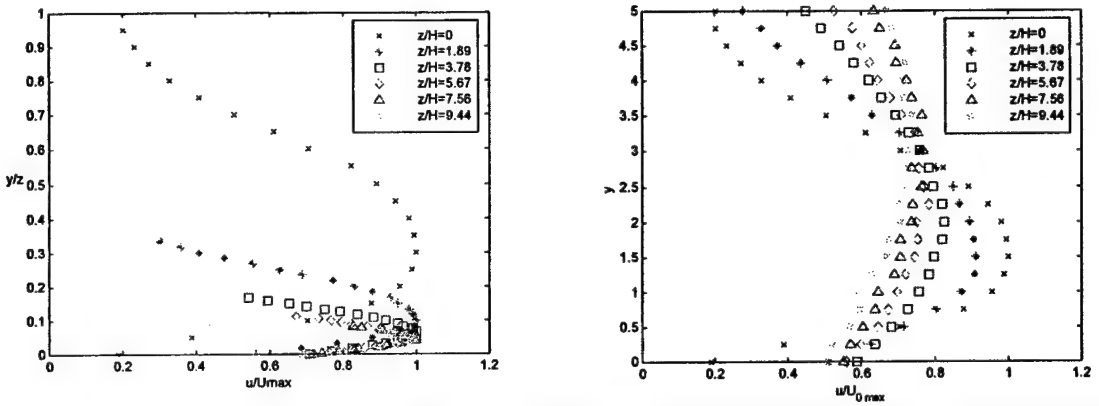

Figure 7: Actuator-jet velocity profiles in self-similar coordinates (left) and actual coordinates (right) Steady Blowing

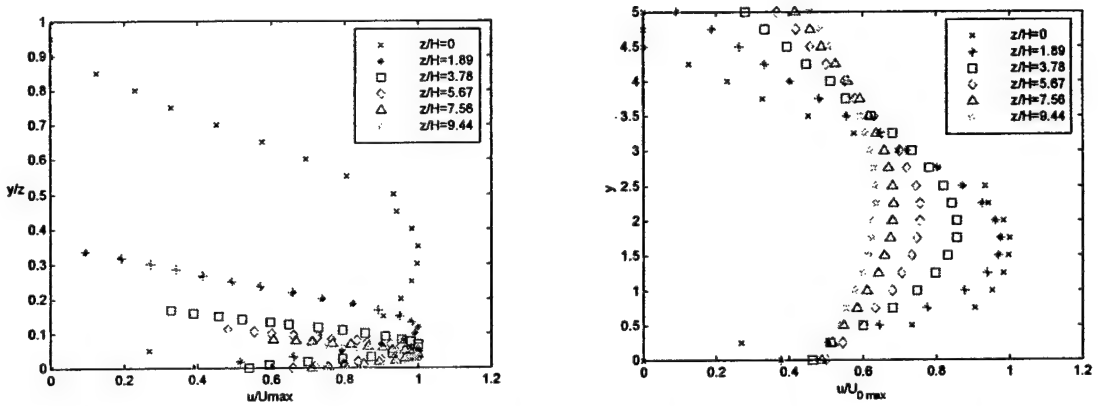

Figure 8: Actuator-jet velocity profiles in self-similar coordinates (left) and actual coordinates (right) 15 Hz

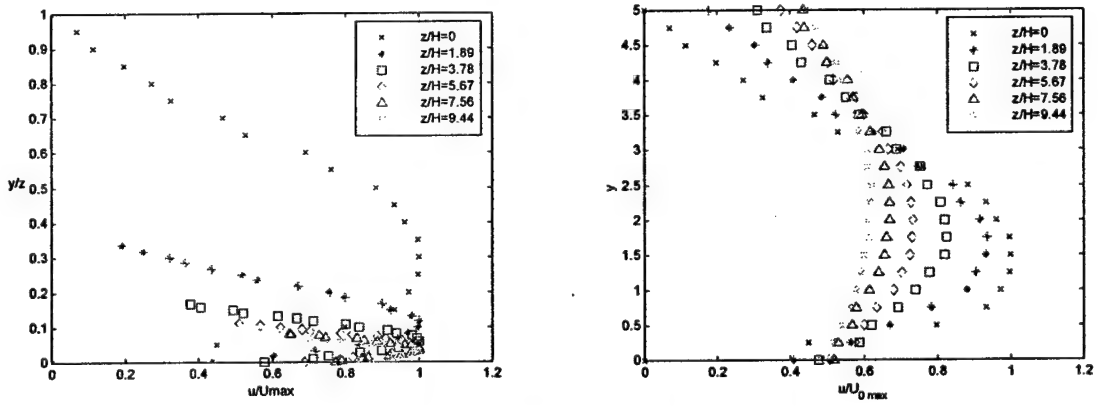

Figure 9: Actuator-jet velocity profiles in self-similar coordinates (left) and actual coordinates (right) 29 Hz

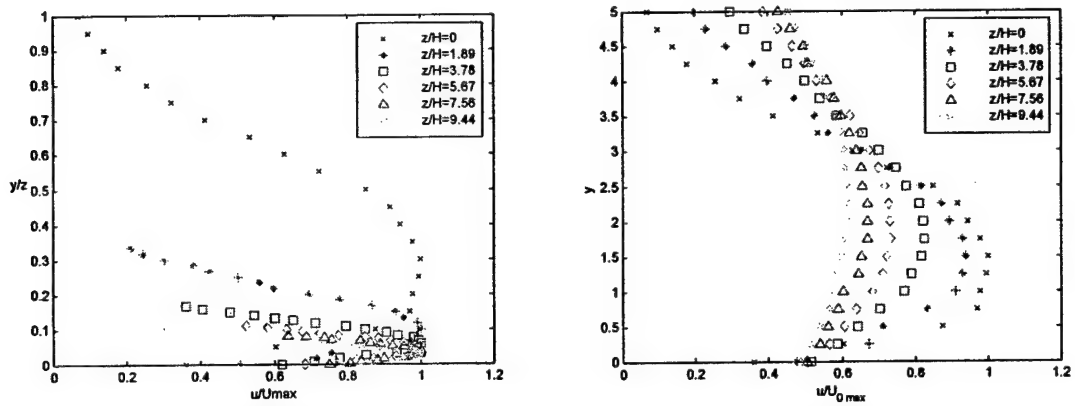

Figure 10: Actuator-jet velocity profiles in self-similar coordinates (left) and actual coordinates (right) 45 Hz

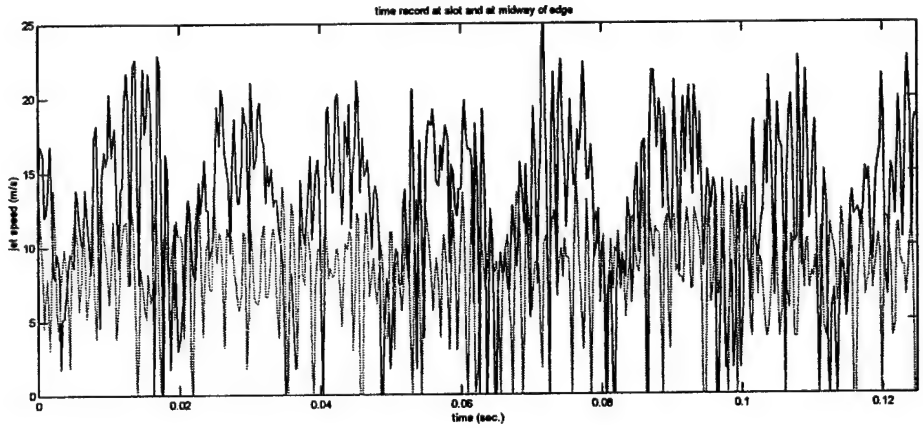

Figure 11: Time records of velocity distributions of the jet for steady (green) and pulsed (blue) blowing .

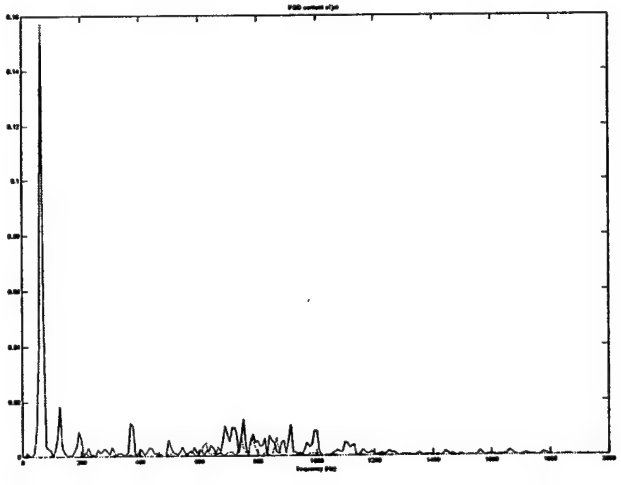

Figure 12:Spectra of velocity distributions of the jet for steady and pulsed motions

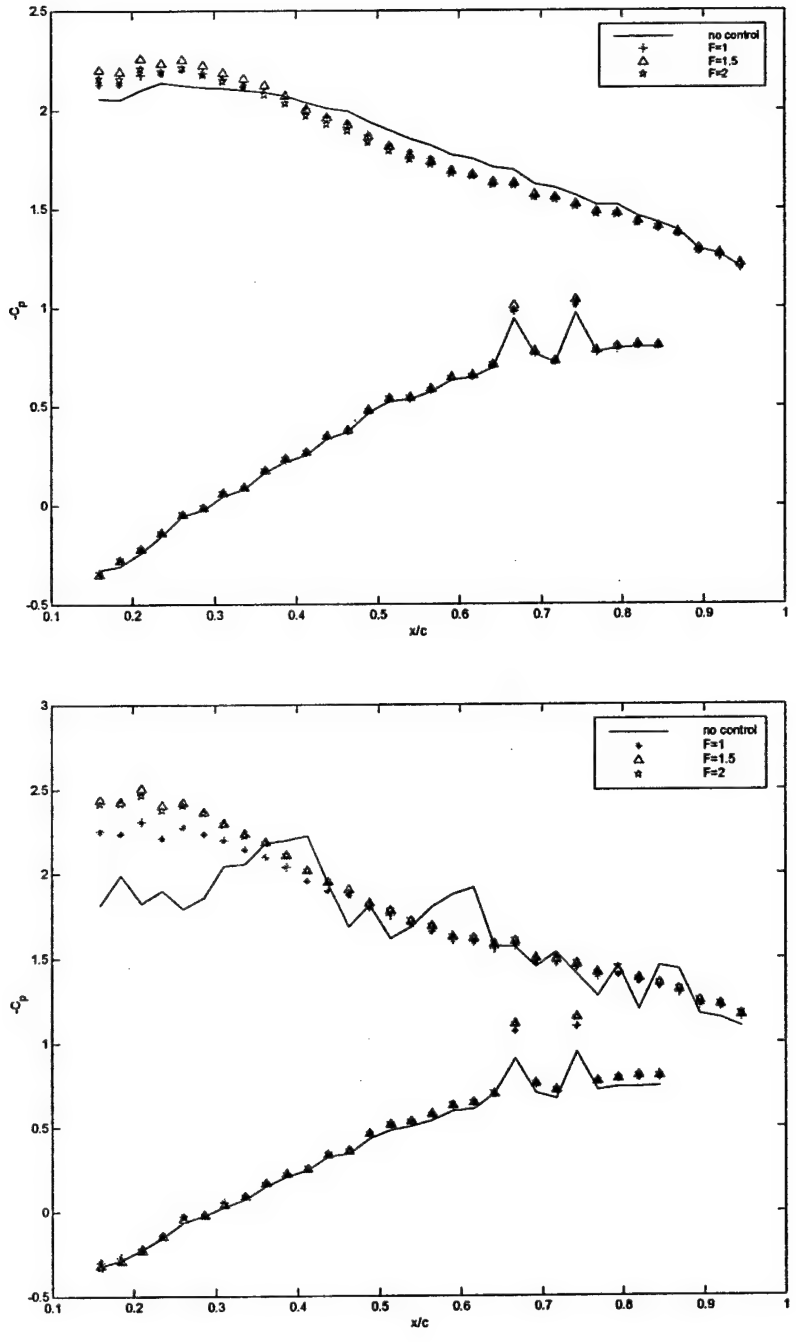

Figure 13: Averaged pressure distributions over the suction and the pressure side of the airfoil for Cμ=0.0175(top) and Cμ=0.03 (top)

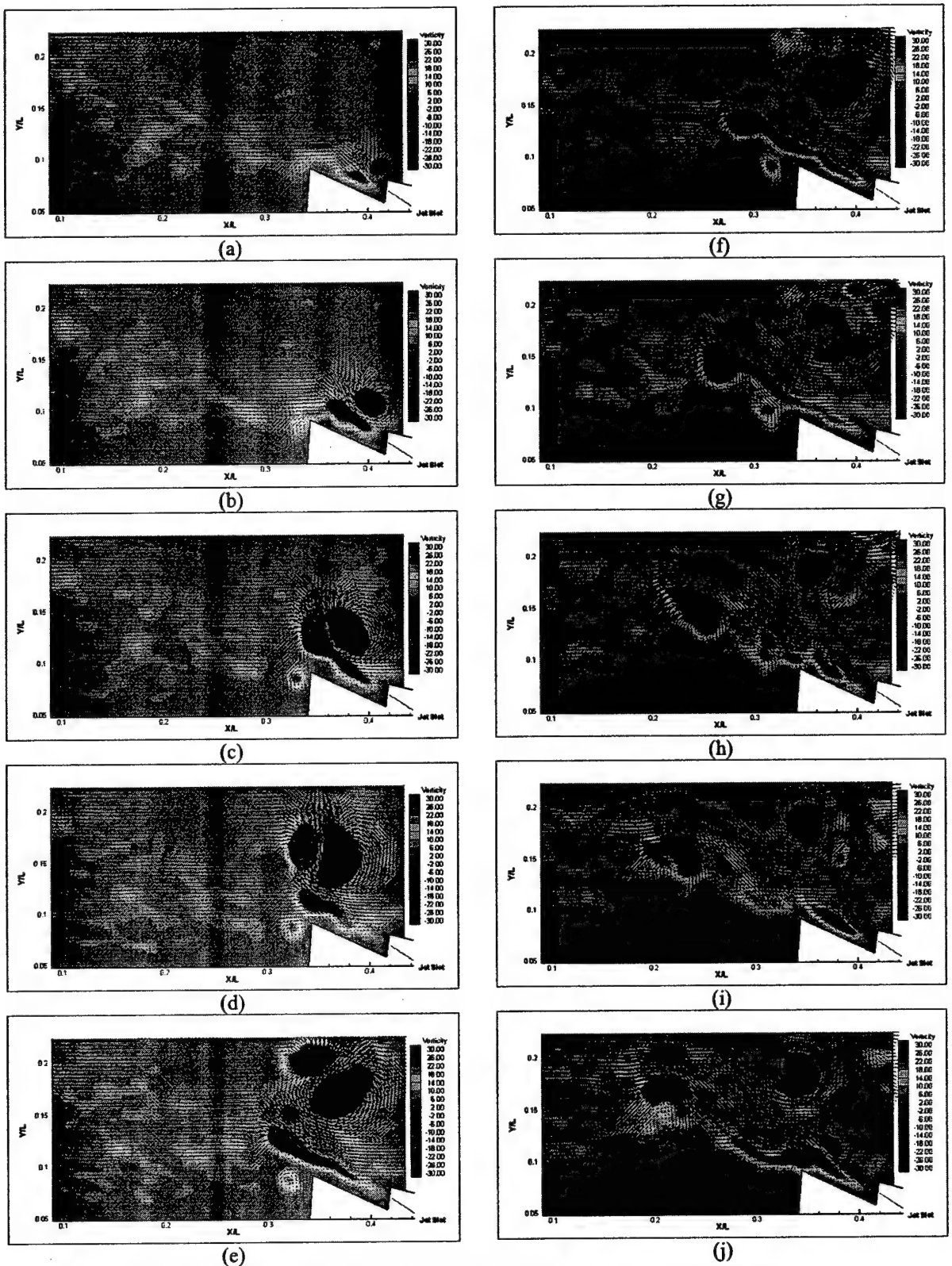

Figure 14: Time sequence of the actuator-jet vorticity contours and velocity distribution flow structure. Dt=0.02 secs

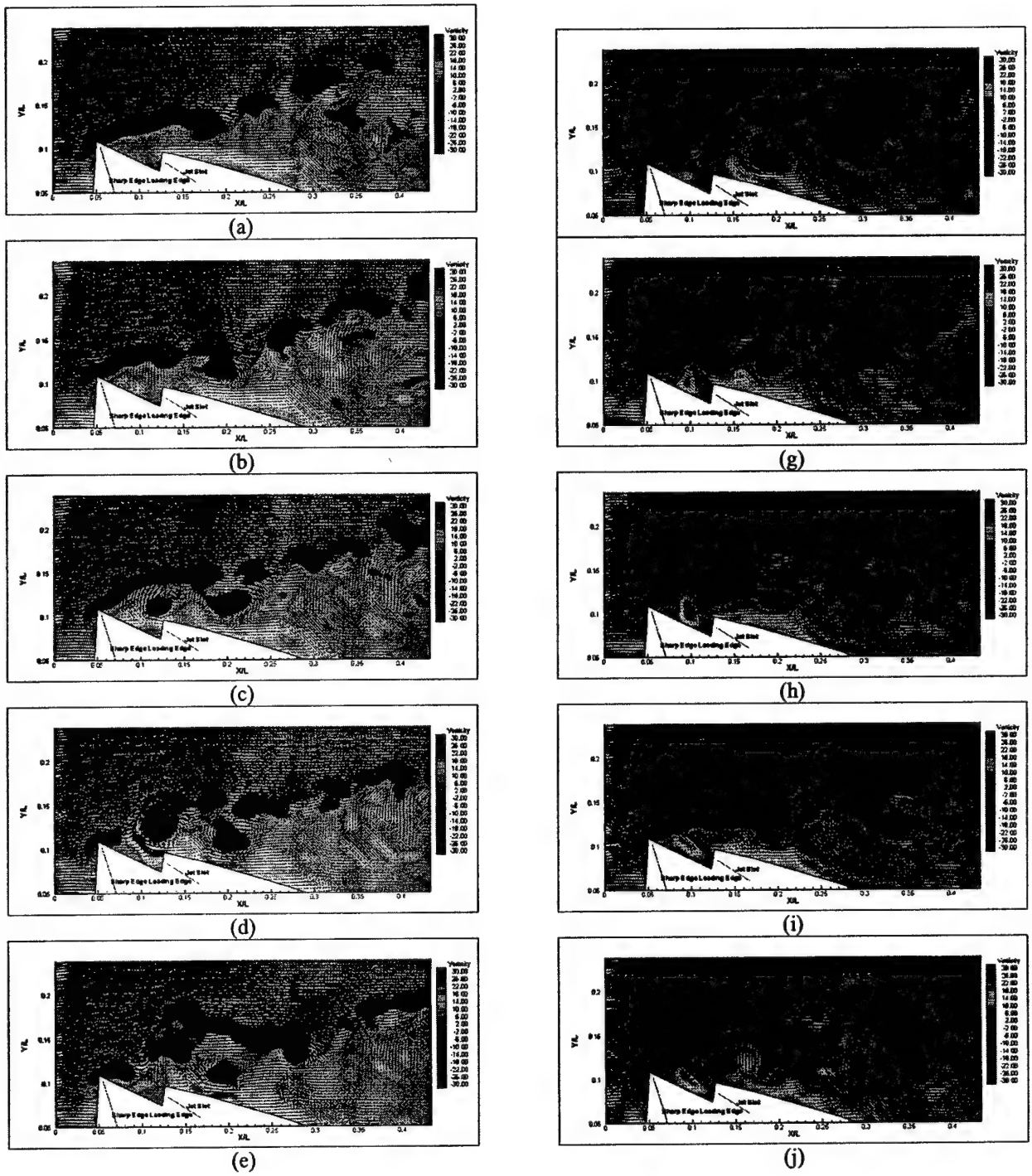

Figure 15:(f) Time sequence of the controlled flow vorticity contours and velocity distribution . Dt=0.02secs

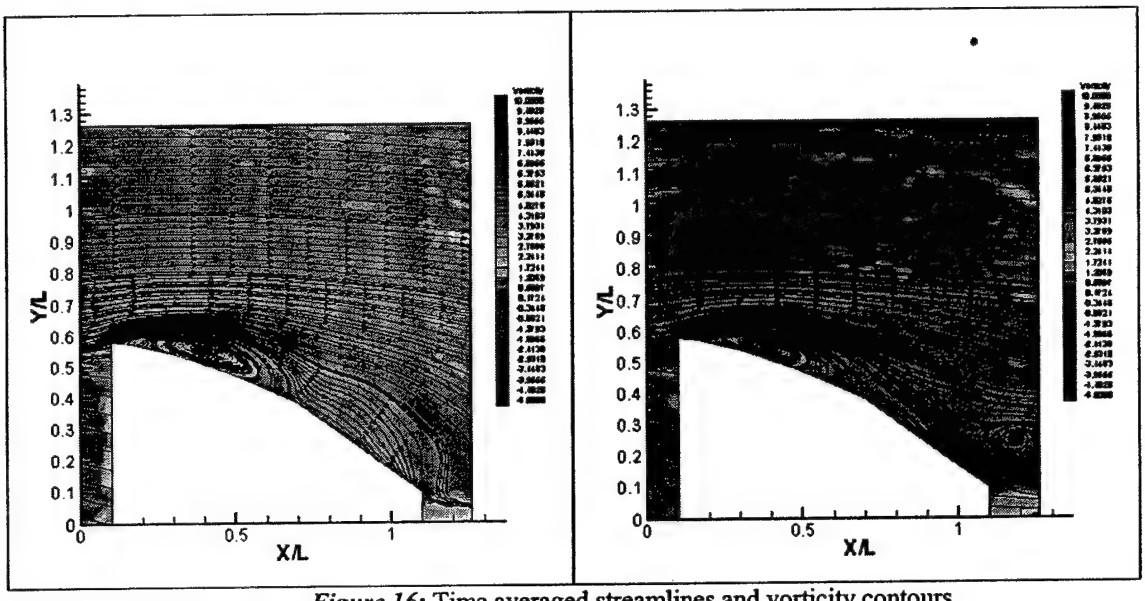

Figure 16: Time averaged streamlines and vorticity contours.
No control-Left. Control-Right

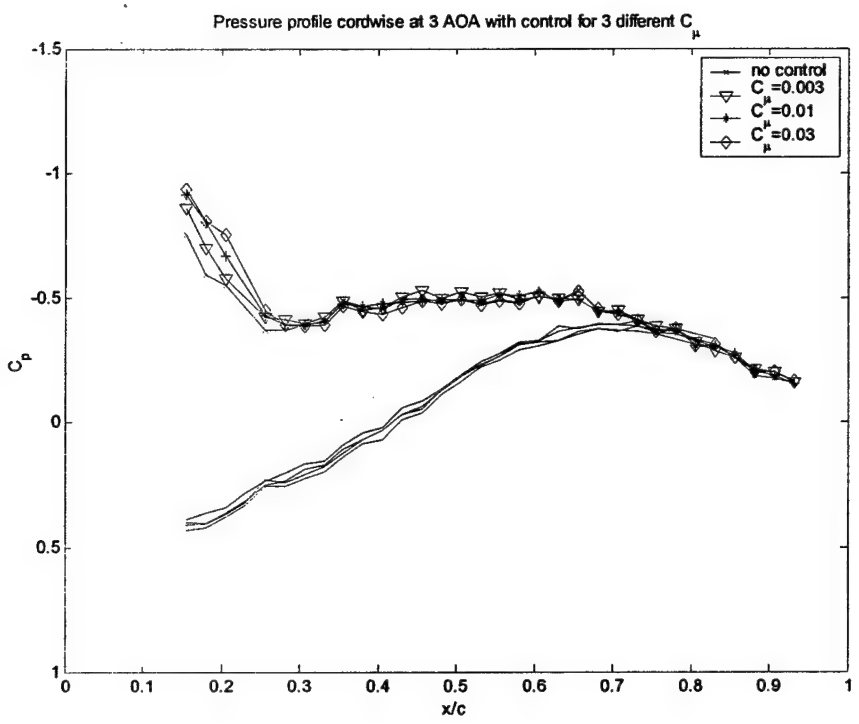

Figure 17:Averaged pressure distributions over the suction and the pressure side of the airfoil for $\alpha=3^0$

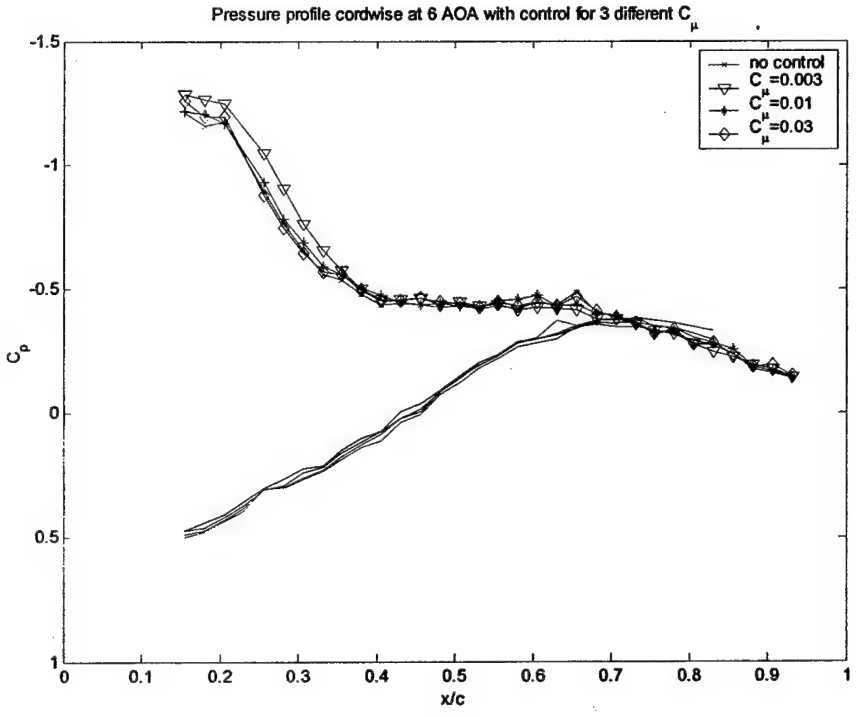

Figure 18:Averaged pressure distributions over the suction and the pressure side of the airfoil for $\alpha=6^0$.

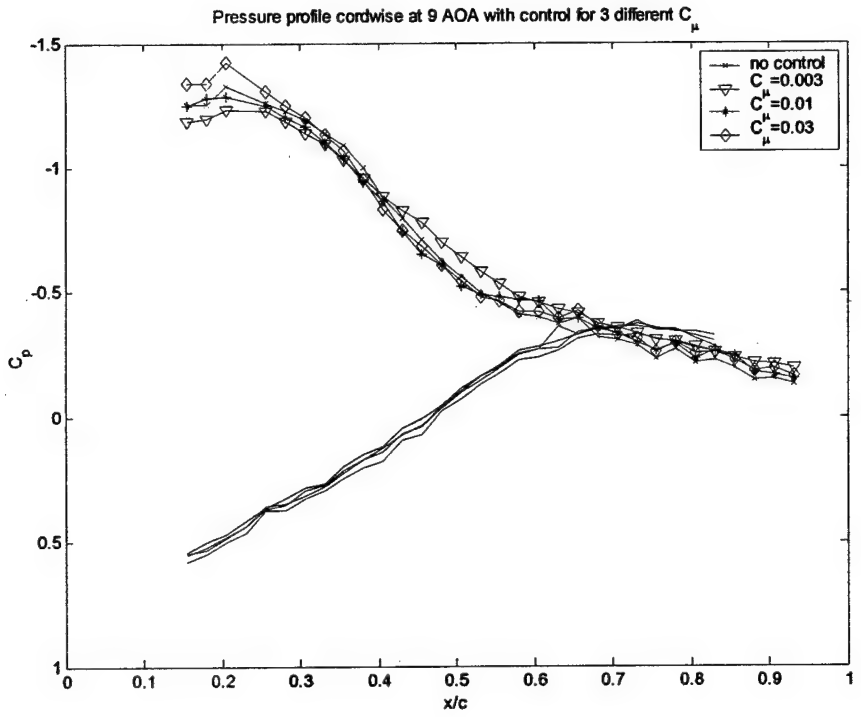

Figure 19: Averaged pressure distributions over the suction and the pressure side of the airfoil for $\alpha=9^0$.

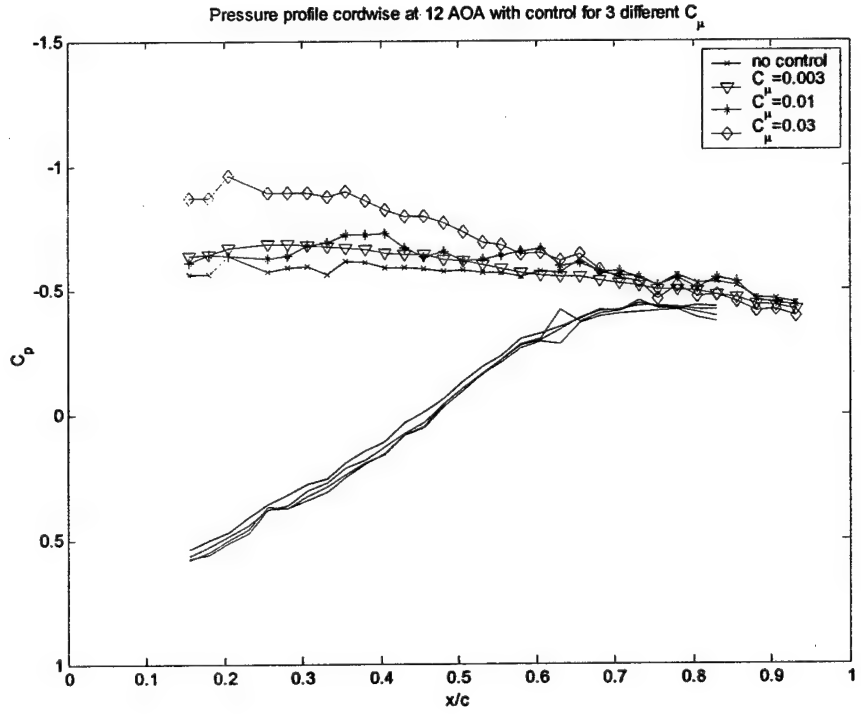

Figure 20: Averaged pressure distributions over the suction and the pressure side of the airfoil for $\alpha=12^0$.

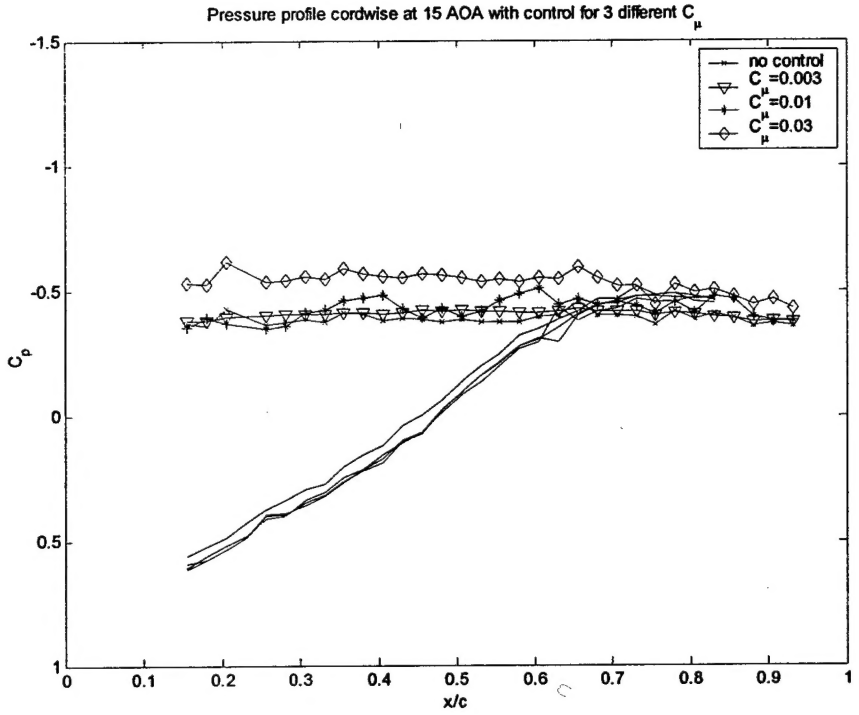

Figure 21: Averaged pressure distributions over the suction and the pressure side of the airfoil for $\alpha=15^0$.

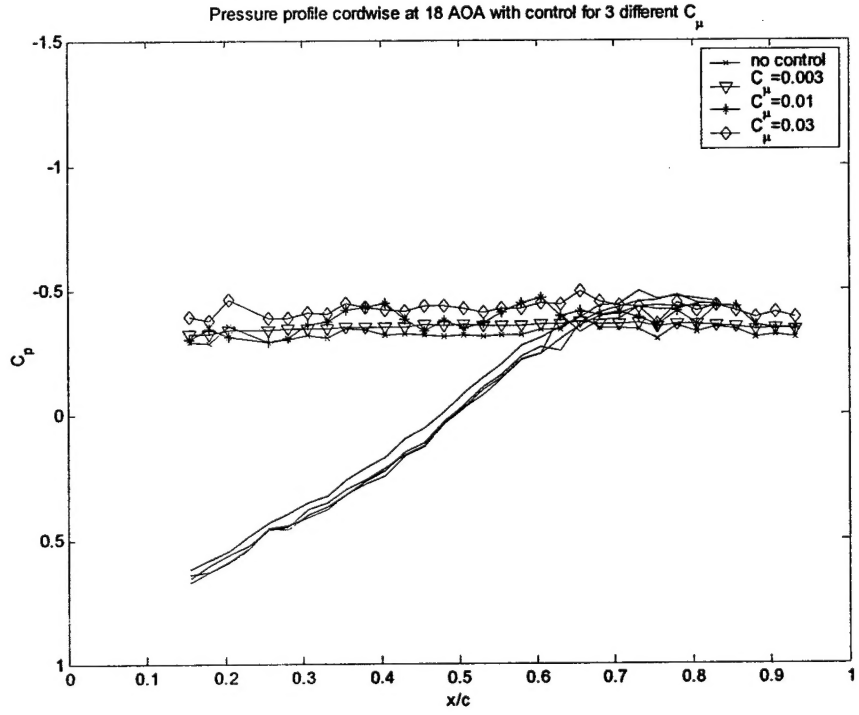

Figure 22: Averaged pressure distributions over the suction and the pressure side of the airfoil for $\alpha=18^0$.

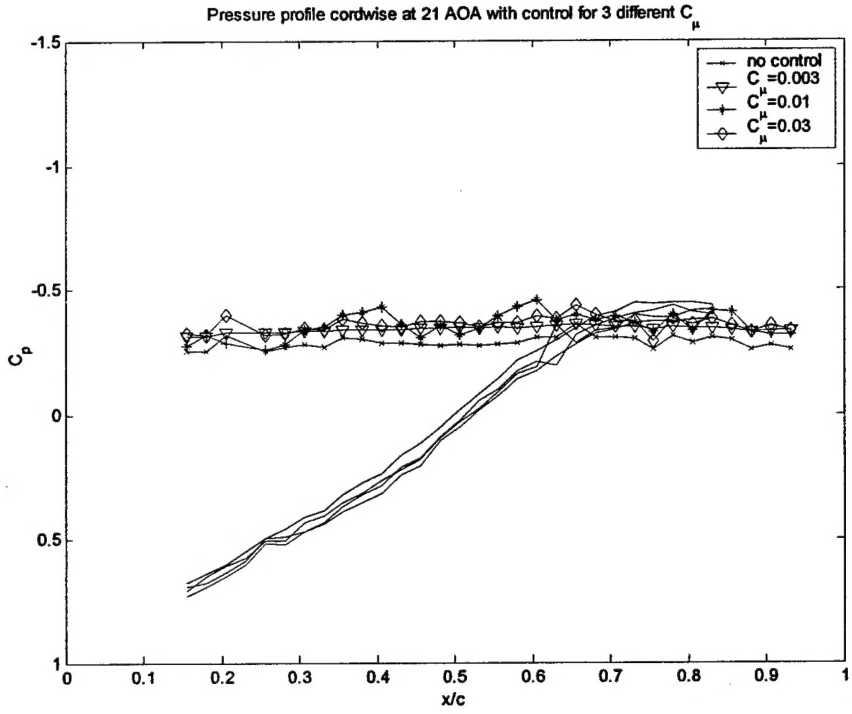

Figure 23:Averaged pressure distributions over the suction and the pressure side of the airfoil for $\alpha=21^0$.

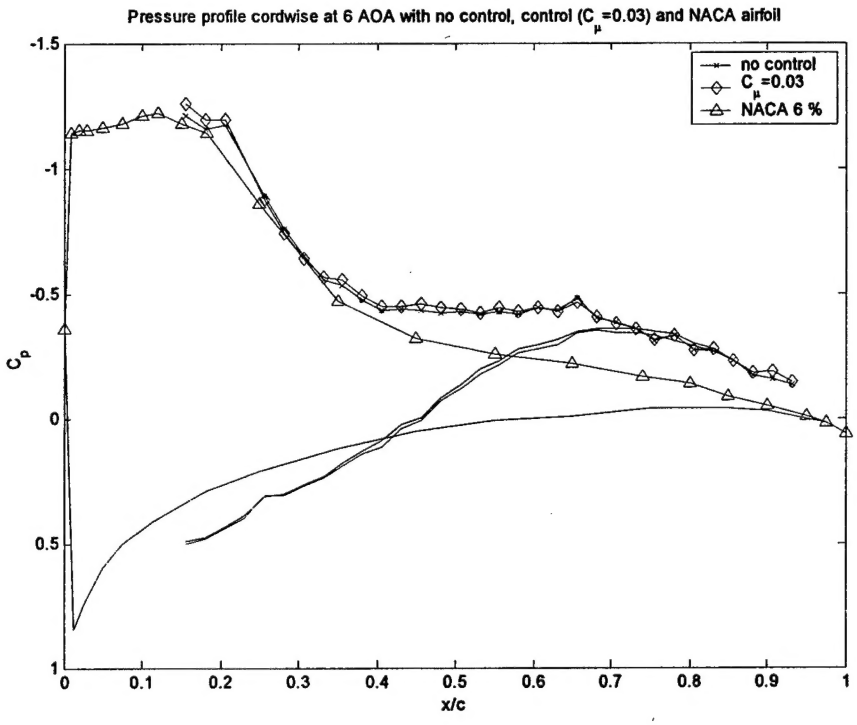

Figure 24: Comparison of present data, controlled and uncontrolled, with the data of Ref. 26, for $\alpha=6^0$.

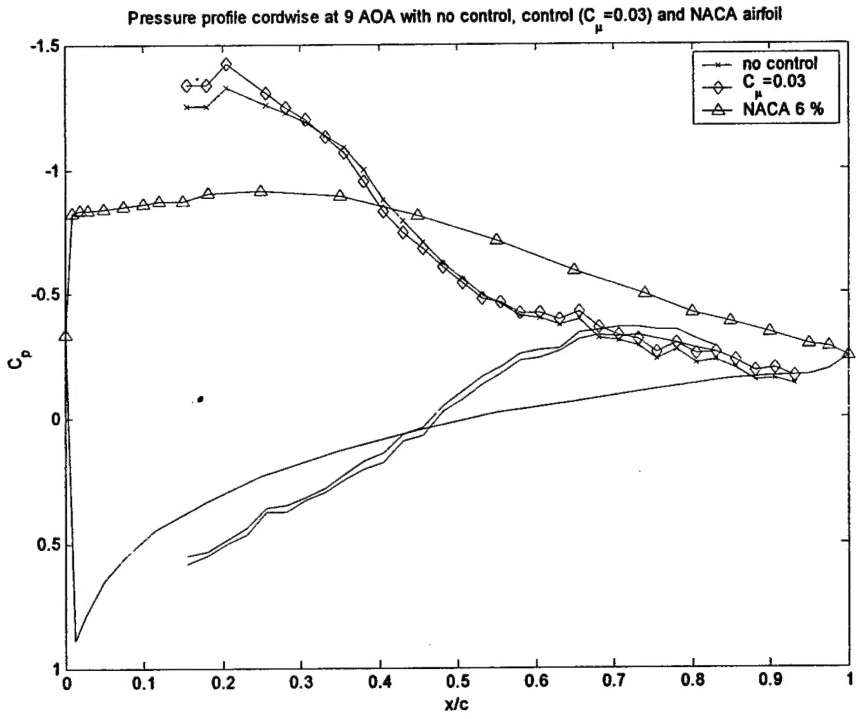

Figure 25:Comparison of present data, controlled and uncontrolled, with the data of Ref. 26, for $\alpha=9^0$.

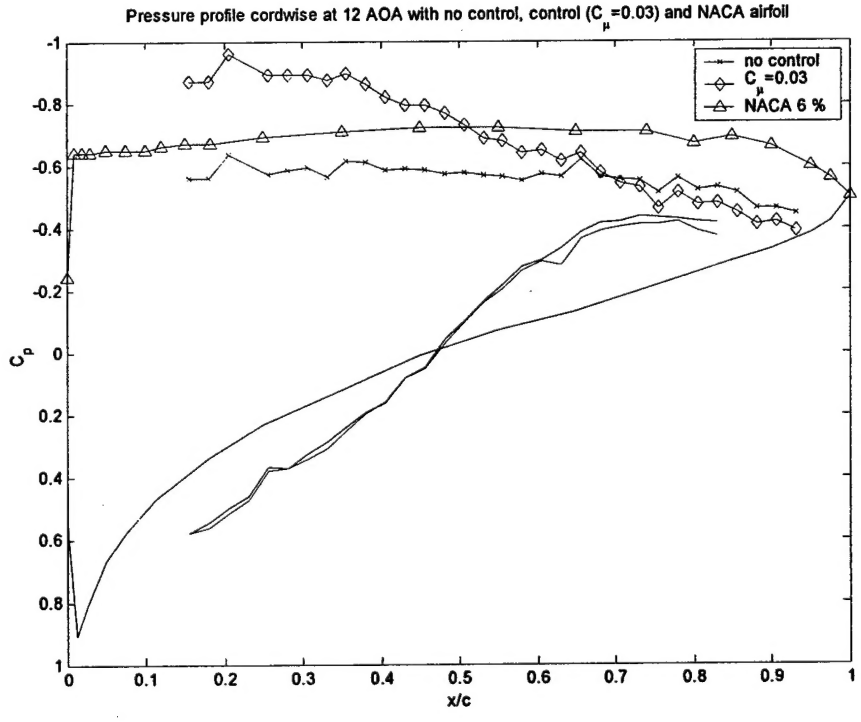

Figure 26:Comparison of present data, controlled and uncontrolled, with the data of Ref. 26, for $\alpha=12^0$.